Journal of Marine Science and Application (2021) 20:10–20
https://doi.org/10.1007/s11804-020-00188-6

RESEARCH ARTICLE

Anticorrosive Properties of Green Silver Nanoparticles to Prevent Microbiologically Influenced Corrosion on Copper in the Marine Environment

Nalan Oya San Keskin[1] · Esra Yaylaci[2] · Selen Guclu Durgun[2,3] · Furkan Deniz[1] · Hasan Nazır[4]

Received: 29 February 2020 / Accepted: 17 September 2020 / Published online: 22 January 2021

Abstract

Microbiologically influenced corrosion is a global problem especially materials used in marine engineering. In that respect, inhibitors are widely used to control fouling and corrosion in marine systems. Most techniques used in inhibitor production are expensive and considered hazardous to the ecosystem. Therefore, scientists are motivated to explore natsural and green products as potent corrosion inhibitors especially in nano size. In this study, antibacterial and anticorrosive properties of green silver nanoparticles (AgNPs) were studied through weight loss, electrochemical characterization, and surface analysis techniques. The corrosion of copper (Cu) in artificial seawater (ASW), *Halomonas variabilis* (*H. variabilis*) NOSK, and *H. variabilis* + AgNPs was monitored using electrochemical measurements like open circuit potential (OCP), electrochemical impedance spectroscopy (EIS), and potentiodynamic polarization curves. AgNPs showed excellent antibacterial activity against pathogenic microorganisms. Electrochemical studies demonstrate a noticeable decrease in OCP and current density in ASW containing *H. variabilis* + AgNPs compared to both ASW and ASW inoculated with bacterium, which confirmed the decrease of corrosion rate of copper. Furthermore, the obtained voltammograms show that the silver nanoparticles were adsorbed on the copper electrode surface from the corrosion solution. Thus, the results prove that the novel idea of green silver nanoparticles acts as an anticorrosive film in the marine environment.

Keywords Antimicrobial · Copper · Electrochemical impedance spectroscopy · Transmission electron microscopy · Microbiologically influenced corrosion · Nanoparticle

Article Highlights
- AgNPs were synthesized from bacteria and used as an anticorrosive inhibitor.
- AgNPs showed excellent antibacterial activity against pathogenic microorganisms.
- Corrosion rate of copper decreased both in ASW and ASW inoculated with bacterium due to AgNPs.

✉ Nalan Oya San Keskin
nalan.san@hbv.edu.tr

[1] Polatlı Science and Literature Faculty, Biology Department, Nanosan Laboratory, Ankara Hacı Bayram Veli University, 06900 Ankara, Turkey

[2] Faculty of Medicine, Department of Medical Biology and Genetics, Gazi University, 06560 Ankara, Turkey

[3] Department of Medical Biology, Lokman Hekim University, 06510 Ankara, Turkey

[4] Faculty of Science, Department of Chemistry, Ankara University, 06100 Ankara, Turkey

1 Introduction

Copper (Cu) is extensively used in aqueous environment, heat exchangers, water cycling systems, and nuclear waste storage systems (Chen and Zhang 2018). Although Cu and its alloys are highly resistant to oxygen corrosion good corrosion resistance and antibacterial properties, still they are vulnerable to microbiologically influenced corrosion (MIC). Many Cu MIC problems and investigations have been reported in the literature (Abdolahi et al. 2014; Chandra et al. 2019; Jia et al. 2019; Preethi et al. 2019).

Due to corrosion and biofouling, materials' service life decrease, which is a serious technological and economic problem especially in the marine environment (Parthipan et al. 2017; Starosvetsky et al. 2007; Xu et al. 2017). Because of the corrosion, around US$4 trillion was lost globally each year (Li et al. 2015).

When metal surfaces submerged in the marine environments, various marine microorganisms such as bacteria, microalga, and their metabolic products attached on the surface of the metal within a few hours and begin to form biofilm (San et al. 2012a; Wang et al. 2004; Videla et al. 1988). Especially, microbiologically influenced corrosion is involved in 50% of all pipeline failures (Wang et al. 2014).

At the metal/biofilm interface, mature biofilm induces changes in the electrochemical conditions such as lowering pH due to secretion of acidic metabolites, reduction of dissolved oxygen due to microbial respiration underneath the biofilm, and localized high concentration of the electrolyte constituents (George et al. 2003; Little and Lee 2007). The process is termed as microbiologically influenced corrosion (MIC). However, biofilm layers sometimes act as a diffusion barrier that decreased corrosion rates via preventing corrosive substance from degrading the metal surface termed microbiologically influenced corrosion inhibition (MICI) (Moradi et al. 2019; San et al. 2012b; Videla and Herrera 2009).

Microorganisms live almost everywhere. In different environments such as marine, oilfield, and soil environment, microbiologically influenced corrosion (MIC) occurs and often results in enormous economic loss and hazardous safety conditions in water environments (Liu and Cheng 2018) and many industries such as oil and gas, water utilities, and medical implant industry (Brauer et al. 2017; Jia et al. 2019). In order to protect metals/alloys from corrosion, coatings and inhibitors have been widely used in the industry (Ou et al. 2018; Poulios et al. 1999). Furthermore, they are rather inefficient. Therefore, there is an urgent need for environmentally friendly and sustainable corrosion control strategies (Kip and Van Veen 2015).

Recently, nanometallic particles have attracted much attention of the scientists due to the varied range of their application in many fields, including optics, electronics, magnetics, catalysis, biomedicine, and so forth (Firdhouse and Lalitha 2015; Huang et al. 2019; Mittal et al. 2014; Otari et al. 2015). Especially, nanoparticles with antimicrobial activity fulfill the general needs of new anticorrosive materials (Baygar et al. 2019). A number of nanoparticles with antimicrobial activities have been reported recently. For this reason, silver nanoparticles as antimicrobial agents have received much attention (Maharubin et al. 2019; San Keskin et al. 2016).

Physical and chemical methods are used for generation of metallic nanoparticles but these methods have low productivity and the chemical methods lead to contamination based on initiator chemicals, use of toxics solvents, and the formation of dangerous by-products (San Keskin et al. 2016). The generation of safe and green chemistry bioprocesses for the synthesis of nanoparticles is an important matter of nanotechnology. Thus, there is an increasing need to improve high yield, confidential, clean, and environmentally friendly methods as the preparation of nanoparticles (Fayaz et al. 2010; Nayak et al. 2011; Thakur et al. 2017). To this end, compared to physical and chemical methods, biosynthesis has appeared as an easy, clean, and applicable approach (Bhaumik et al. 2016). Many reports on the synthesis of silver nanoparticles using bacteria drew the most interest in this area (Cao 2017). Using bacteria has one benefit for biosynthesis of nanoparticles due to ease of handling and their manipulation simply (Fayaz et al. 2010; Hebbalalu et al. 2013). There have been studies demonstrating that cell-free extracts of some bacterial species, like *Escherichia coli* and *Klebsiella pneumoniae* (Shahverdi et al. 2007), could encourage the synthesis of silver nanoparticles.

In the present work, green silver nanoparticles were synthesized from bacteria and used as biocorrosion inhibitors in order to improve the corrosion resistance of copper in marine environment influenced by halophilic bacterium, *H. variabilis*.

2 Material and Methods

2.1 Chemicals

The chemicals used in this experiment are silver nitrate ($AgNO_3$), LB broth (Luria-Bertani), nutrient broth (NB), and nutrient agar (NA) obtained from Sigma-Aldrich. Other chemicals used were of analytical grade.

2.2 Preparation of *Lysinibacillus* sp. NOSK Cell-Free Extract for AgNPs Production

Strain was isolated from soil samples collected from the Ankara River at 6-in depth from surface on the NA plate supplemented with 5.0% methanol. The isolate was characterized as *Lysinibacillus* sp. with the molecular identification and later is named as *Lysinibacillus* sp. NOSK, which was stored in GenBank with KM241862 accession number (San Keskin et al. 2015). To prepare *Lysinibacillus* sp. NOSK cell-free extract, a single clone of the isolate was transferred from the Luria-Bertani (LB) agar plate into 50 ml of sterile nutrient broth (NB) in a 100-ml Erlenmeyer flask. The flask was incubated at 30 °C for 48 h on a rotary shaker (E 20/60, Biosan Latvia) at 100 rpm. After the incubation period, when the culture OD at 600 nm was between the ranges of 1 and 2, the cell-free extract recovered by centrifugation (4000 rpm, 10 min at room temperature) and was used for further experiment.

2.3 Preparation of *H. variabilis* NOSK for MIC Analysis

Extremophiles are microorganisms that grow under conditions hostile to most organisms. Some of them, such as *Halomonas* bacterium which thrive in hypersaline environments, have been recognized for their potential use in

biotechnological applications (Ye et al. 2020). In hypersaline environments, ordinary bacteria can hardly survive but halophilic bacteria are frequently found in marine environment. For this reason, in this study, halophilic bacteria are isolated and identified genetically and investigated MIC in marine environments.

Brine, multicolor solar salt, saline soil, and saline mud samples were collected from Salt Lake, Turkey (39° 05′ 13.1″ N, 33° 23′ 37.8″ E). Samples were collected in sterile plastic containers and were cultured not later than 18 h after collection. All samples were cultured in a saline nutrient broth with a final concentration of 3.5% sea salt. Cultures were incubated at 30 °C in an orbital shaker, at 150 rpm. After 7 days, resultant colonies were purified by repeated streaking on complete media agar. The isolates were stored at 4 °C. Genetic characterization of the isolated bacterium was made on the basis of 16S rRNA. After phylogenetic analysis, sequence data are submitted to GenBank with the accession number of KX351792 (https://www.ncbi.nlm.nih.gov/nuccore/KX351792.1).

For bacterium enrichment, LB medium (10 g/L tryptone, 5 g/L yeast extract, 10 g/L NaCl in 1 L of distilled water) with 3.5% NaCl was used. In addition, incubation conditions were at 30 °C for 48 h on a rotary shaker at 100 rpm. The electrochemical experiments are performed in ASW inoculated with a 1% v/v 24 h bacterial culture (~ 10^9 CFU/mL) (San et al. 2012a).

2.4 Biosynthesis of AgNPs by *Lysinibacillus* sp. NOSK Cell-Free Extract

For the biosynthesis of AgNPs, 10 ml of the cell-free extract was added to 90 ml of 1 mM $AgNO_3$ solution in a 100-ml Erlenmeyer flask (pH 8), which was incubated at 37 °C on the orbital shaker set at 150 rpm in the dark. In our study, the change in the color of the mixture from pale yellow to brownish yellow after 6 h was observed and the color was darkened during the 72-h incubation period.

2.5 Characterization of Biogenic AgNPs

2.5.1 UV-Visible Spectroscopic Analysis

The absorption spectra of the samples taken at different time intervals of incubation were recorded by UV-Vis spectrophotometer (Shimadzu UV1200, Japan) at a resolution of 1 nm in a wavelength range between 300 and 750 nm using a 96-well plate.

2.5.2 Size Distribution and Zeta Potential Analysis

The average particle size distribution and zeta potential of AgNPs in colloidal solution were determined by using Zeta Sizer Nano Series (Malvern Instruments, ZEN 3600). The results were collected in ultrapure water at 25 °C and 173° backscatter angle. The electrophoretic mobility of the nanoparticle solution (1 mg mL^{-1}) was analyzed. Data was altered to zeta (ζ-) potential and size values with the Helmholtz-Smoluchowski equation.

2.5.3 Nanoparticle Characterization

Biosynthesized AgNPs are analyzed to find out the presence of functional groups on the silver nanoparticles via ATR-FTIR spectroscopy. The samples were completely freeze-dried by Christ Alpha Freeze Dryer (Germany) at − 55 °C and the powders were subjected to FTIR measurement. The spectra were recorded by ATR-FTIR (Shimadzu, IRAffinity-1S model, with a DLATGS detector, diamond plate, Japan), in transmittance mode within the range of 400–4000 cm^{-1} with 64 scans at a resolution of 4 cm^{-1}.

2.5.4 Transmission Electron Microscopy

The shape of silver nanoparticles is determined using transmission electron microscopy (TEM). AgNPs' colloidal solution is dropped onto copper TEM grids and measurements are taken at an accelerating voltage (100–200 keV) (FEI HR-TEM).

2.5.5 Antimicrobial Activity of AgNPs Against Pathogens

Four bacterial strains, namely, *Bacillus subtilis* (ATTC 6633), *Staphylococcus aureus* (ATTC 6338), *Escherichia coli* (ATTC 8739), and *Klebsiella pneumoniae* (ATTC 700603), are provided from American Type Culture Collection (ATCC), USA. All bacteria strains are commonly found in hospital-acquired infections. The cultures of *B. subtilis*, *S. aureus*, and *E. coli* were grown in LB at 37 °C for overnight incubation on the orbital shaker at 100 rpm and the culture of *K. pneumoniae* was also grown in LB at 37 °C for 48 h. These cultures were maintained in LB agar plate by continuous subculturing from time to time.

The antimicrobial activity of biosynthesized AgNPs is determined by colony forming unit (CFU) method and well diffusion method. In CFU method, the different concentrations of AgNPs (65 nM, 130 nM, 195 nM, and 260 nM) were added to sterile LB broth and inoculated separately with freshly grown *Staphylococcus aureus* (ATTC 6338), *Bacillus subtilis* (ATTC 6633), *Klebsiella pneumoniae* (ATTC 700603), and *Escherichia coli* (ATTC 8739). After incubation period, the inoculum was diluted and spread uniformly onto the individual plates. All the plates are incubated at 37 °C and at the end of inoculation time, bacterium was counted. In well diffusion method, the cultures of organisms were inoculated to LB agar which are

sterilized and cooled approximately 40–50 °C and were poured into petri dishes. After completely cooled, wells of 5-mm diameter were made on LB agar plate using gel puncture. The different concentrations of AgNPs (65 nM, 130 nM, 195 nM, and 260 nM) are filled into each well on all plates. After incubation at 37 °C, the variable levels of zone of inhibition are evaluated.

2.5.6 Growth Effect of AgNPs Against Corrosion Bacterium *Halomonas variabilis* NOSK

Bacterial growth after 5 h in the corrosion setup was measured by counting (CFU) method. The growth inhibition percentage was obtained with respect to the positive control.

2.5.7 In vitro Cytotoxicity of AgNPs

AgNPs have gained access into our daily life, and the inevitable human exposure to these nanoparticles has raised concerns about their potential hazards to the environment, health, and safety in recent years. For this reason, cytotoxic activities of biosynthesized AgNPs against HeLa cell lines were studied. HeLa cell line which is the cervical cancer cell line was grown in Dulbecco's Modified Eagle Medium supplemented with 10% fetal bovine serum (FBS), 100 μg/mL penicillin, and 100 μg/mL streptomycin at 37 °C in a humidified atmosphere of 95% air and 5% CO_2. For reproduction, 70%–80% of confluence and a density of 2×10^3 cells per well in 96-well plate are incubated for 24 h in 95% air and 5% CO_2 incubator. 3-(4,5-dimethyl-2-thiazolyl)-2,5-diphenyl-tetrazolium bromide (MTT) assay is used for the determination of the cytotoxic activity of biosynthesized AgNPs against HeLa cell lines. Different concentrations of the AgNPs in distilled water are added and incubated for 24 h at 5% CO_2 incubator. After incubation, 10 μL (5 mg/mL in PBS) of MTT was added to each well and incubated for 4 h at 37 °C. The resulting formazan was dissolved in 200 μL of DMSO and the viable cells were determined by measuring the absorbance at 570 nm. The concentration of AgNPs showing 50% inhibition of viability (IC_{50} values) was determined. The percentage of viability was calculated as the following formula:

$$\text{viable cells}\% = \frac{A570 \text{ of AgNP treated sample}}{A570 \text{ of untreated sample}} x\ 100 \quad (1)$$

2.6 Weight Loss Measurements

The corrosion rates of disks which have 0.5 cm^2 exposed area were monitored by weight loss technique. The weight loss was determined at 25 °C by weighing the cleaned samples before and after the copper disk in the ASW with the absence and presence of bacterium and AgNPs. The coupons were removed from the environments at the interval of 5 h; the cleaning procedure consisted of wiping the disks with a paper tissue and washing with distilled water and acetone, followed by oven drying at 80 °C. The rate of the corrosion was calculated based on the equation given below:

$$\text{Corrosion rates} = \frac{(K\ x\ W)}{(A\ x\ T\ x\ D)} \quad (2)$$

where K is a constant, T the time of exposure in hours, A the area in cm^2, W is the mass loss in g, and D is the density of copper in g/cm^2 (Liu et al. 2019).

2.7 Electrochemical Studies

Electrochemical analysis was conducted at room temperature in ASW which contained (g/L) 26.29 NaCl, 0.74 g KCl, 0.99 g $CaCl_2$, 6.09 g $MgCl_2$ $6H_2O$, and 3.94 g $MgSO_4 \cdot 7H_2O$ and adjust the pH to 7.8 and store at 4 °C. 1 g/L concentration of glucose is added to the media as carbon and energy sources. In our three different corrosion analysis setup, the copper electrodes are placed in artificial seawater under sterile conditions, in the presence of *H. variabilis* NOSK and bacterium with AgNPs. In the setups, cell number in the bacterial solution was determined based on the standard calibration with the assumption that an OD600 nm value of 1.0 is equivalent to 10^9 cells/mL.

EIS studies were conducted using CH Instruments Inc., USA (Model CHI-608E), with a traditional three-electrode cell with a capacity of 90 mL, with platinum as the counter electrode, an Ag/AgCl (3 M KCl) as the reference electrode, and copper disk (0.5 cm^2 exposed area) as the working electrode. First, working electrode is polished with abrasive paper (400, 600, 800, and 1200 grade) and then cleaned with ethyl alcohol. At the end, in order to sterilize the samples, all the samples are exposed to ultraviolet (UV) light for 30 min. In addition, we confirmed the surface film formed by AgNPs after 5-h corrosion test with their electrochemical behavior in 50-mM phosphate buffer (pH 7.4) using cyclic voltammetry (scans originating at 100 mV/s (vs. Ag/AgCl) (Giovanni and Pumera 2012).

2.8 Statistical Analysis

ZSimpwin and EISSA data analysis software were used to fit the EIS data. All the measurements were recorded in triplicate and the results are expressed as means ± the standard errors of the means.

3 Results and Discussion

3.1 Characterization of the Biogenic AgNPs

The reduction of aqueous $AgNO_3$ solution is a largely used method for biosynthesis of AgNPs (Mittal et al. 2014). The first characterization analysis of the biosynthesized AgNPs is performed by using UV-Vis spectroscopy. Figure 1a shows the UV-Vis absorption spectra recorded from aqueous $AgNO_3$—the cell-free extract of the *Lysinibacillus* sp. NOSK medium as a function of time of reaction. Inset shows the UV-Vis close look for the spectra of AgNPs at 1- to 8-h time intervals. After 6-h incubation, the color of the reaction mixture began to change that indicates more than 6 h required for the synthesis of detectable amount of AgNPs (Figure 1b). After 24 h, the light yellow color change to yellowish brown color; that is, the typical optical property of AgNPs' color shows the formation of nanoparticles. The density of the color of reaction mixture was directly proportional to the time of incubation. In addition, the characteristic surface plasmon resonance (SPR) peak of the mixture was between 420 and 430 nm, demonstrating the presence of AgNPs. The SPR spectra suggest that these AgNPs are spherical in shape (Gou et al. 2015; Otari et al. 2015).

In Figure 1, the inset shows the UV-Vis spectrum of AgNPs at 1- to 8-h time intervals. DLS data represent an average particle size and particle size distribution. The average particle size of the samples taken at different time intervals of incubation (30 min, 1 h, 2 h, 3 h, 4 h, 5 h, 6 h, 8 h) is almost identical (Figure S1) and after 24 h of reaction, the size of the nanoparticles began to increase. From Figure 2a, it shows 42 nm was the average particle size distribution of AgNPs in colloidal solution for 24 h and 0.166 polydispersity index (PDI) was obtained. From Figure 2b and Figure 2c, it indicates that the average size values recorded for 48 h and 72 h are 61 nm and 76 nm, respectively. Thus, the particle size increase formed as time progressed can be associated with agglomeration.

The zeta potential measurement is an important demonstration of the stability of nanoparticles in colloidal solution. High absolute zeta potential ($\xi > \pm 30$ mV) attributes to a high electric surface charge on the AgNPs which can lead to strong repulsive power among the nanoparticles to prevent them from aggregation. The negative zeta potential of − 23.1 mV is observed for 24 h that the capping molecules existing on the surface of AgNPs frequently contained negatively charged groups and are responsible for the stability (Table S1) (Arulmozhi et al. 2013).

Figure 3 shows the vibrations of the amide I and amide II bands of the proteins of the sample for 24 h (Kardas et al. 2014). The absorbance at 3619 cm^{-1} and 3736 cm^{-1} attributed to O-H stretching vibration modes of hydroxyl functional group and N-H stretching vibration modes of amino functional group in proteins (Gou et al. 2015). The other bands such as 2923 cm^{-1}, 2851 cm^{-1}, and 1741 cm^{-1} can be related to CH_2 asymmetric stretching and CH_2 symmetric stretching of mainly lipids from proteins, nucleic acids and carbohydrates, and C=O stretching of triglycerides and cholesterol esters. All these functional groups may have an efficient role in the biosynthesis of AgNPs. It indicates that the release of extracellular

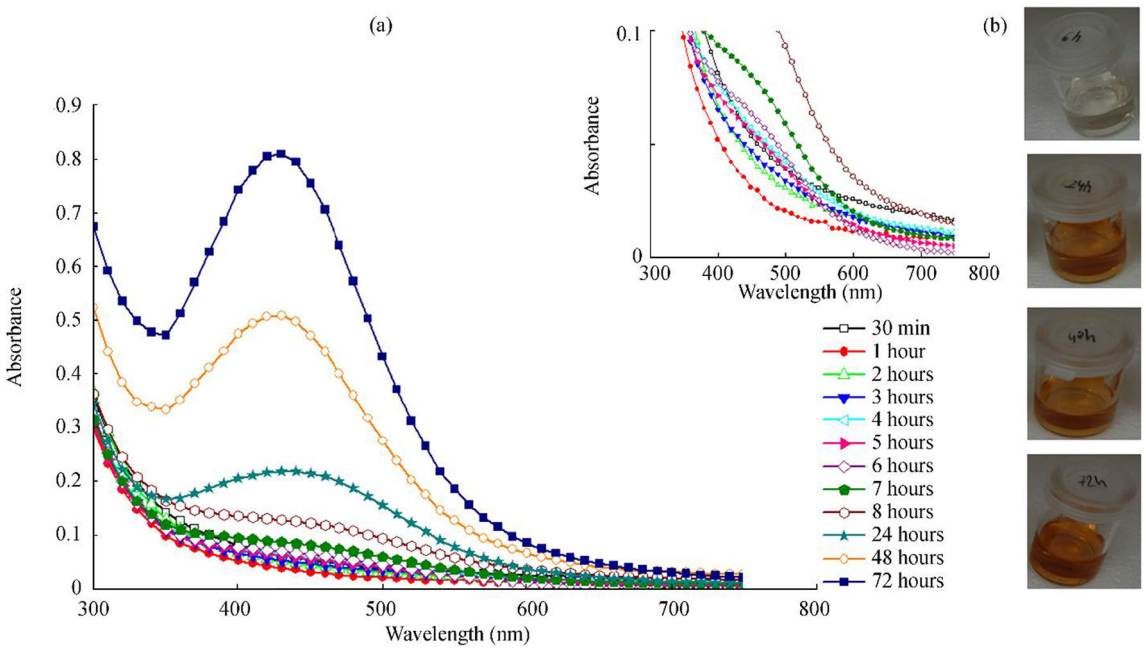

Figure 1 (**a**) UV-Vis absorption spectra of silver nanoparticles. (**b**) The color change of the reaction mixture

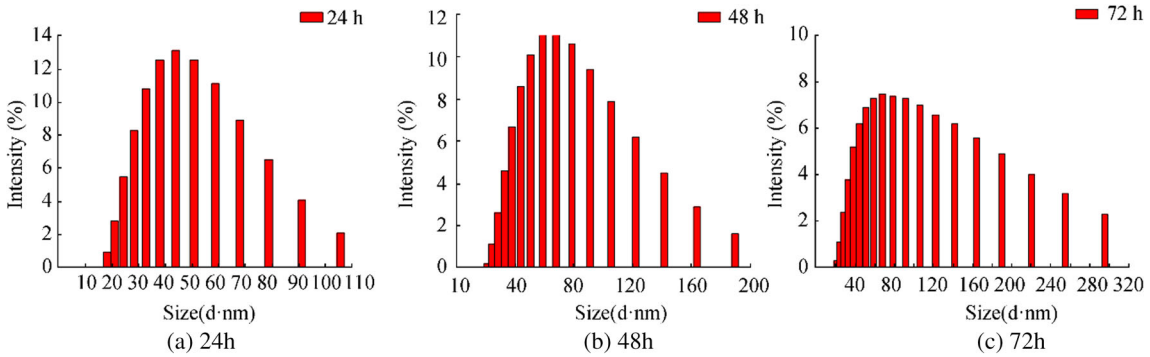

Figure 2 Histogram of silver nanoparticle distributions. (**a**) 24 h, (**b**) 48 h, and (**c**) 72 h

biomolecules could probably perform the function of the formation and stabilization of AgNPs in colloidal solution (Fayaz et al. 2010).

The TEM micrographs of the biosynthesized silver nanoparticles are shown in the Figure 4a, 4b, and 4c with 50, 5, and 2 nm scales, respectively. As seen in the TEM micrographs, synthesized AgNPs were spherical in shape. Furthermore, the selected area electron diffraction (SAED) patterns reveal that the particles are crystalline in nature (Figure 4d).

3.2 Antimicrobial Activity and In vitro Cytotoxicity of AgNPs

Silver has been utilized for many years in the field of medicine for bactericidal applications due to antimicrobial properties (Firdhouse and Lalitha 2015). Although the antimicrobial effects of the biosynthesized AgNPs are shown in several studies, the exact mechanism remains to be unexplained (Kim et al. 2007). Most studies showed that the surface of the negatively charged bacterial cell membrane may attract positively charged AgNPs and interact with structural elements of the bacterial cell membrane, which may lead to structural changes disturbing permeability and respiration functions of the cells and finally cell death (Sondi and Salopek-Sondi 2004). Kim et al. (2007) reported that the free radical consisted of metal depletion from the surface of AgNPs may be responsible for antimicrobial activity which is known to destroy the cell membrane integrity. Moreover, particle dimension and shape may affect the bactericidal activities of AgNPs. The smaller AgNPs, which have large surface areas for interactions, would demonstrate more antibacterial efficacy than the larger AgNPs. This has been facilitated to interact with the cell wall of the bacterium and cause death of the cells (Kailasa et al. 2019).

In the present study, the biosynthesized AgNPs showed antimicrobial activity against Gr(+) *Staphylococcus aureus* and *Bacillus subtilis* and Gr(−) *Klebsiella pneumoniae* and *Escherichia coli* dependent on the concentration of AgNPs (Peszke et al. 2016). In CFU method, the number of bacterial

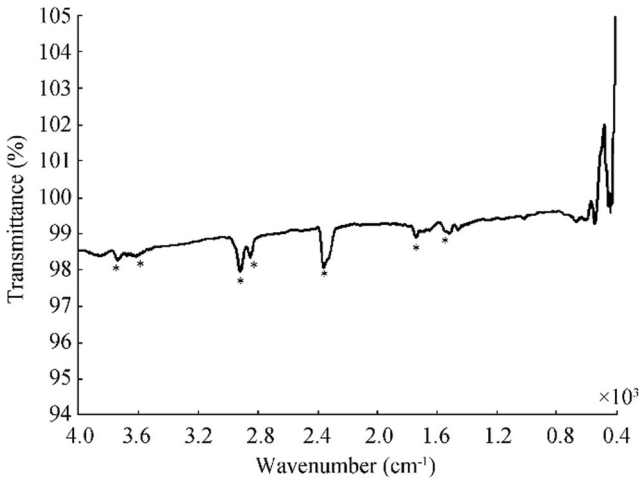

Figure 3 FTIR spectrum of the freeze-dried sample containing AgNPs

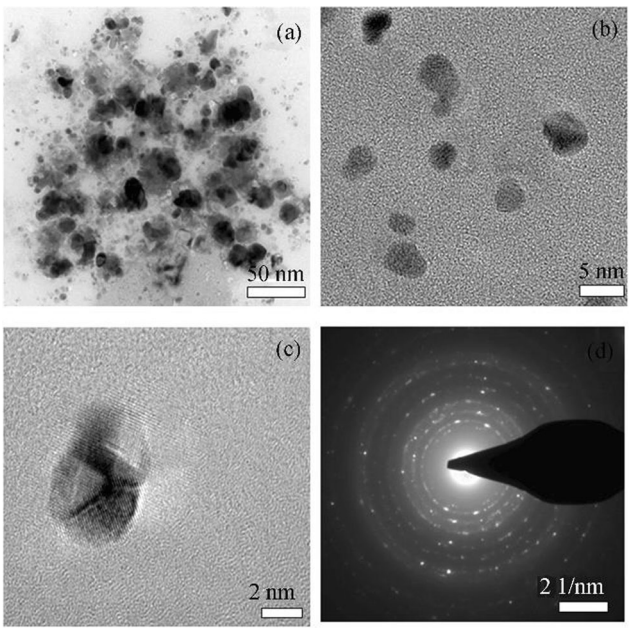

Figure 4 TEM micrograph of the biosynthesized silver nanoparticles. (**a**) 50, (**b**) 5, and (**c**) 2 nm scales, and (**d**) the selected area electron diffraction (SAED) patterns

colonies reduced with the increasing of the concentration of AgNPs. The growth inhibitory rates at different concentration of AgNPs with 65 nM, 130 nM, 195 nM, and 260 nM are calculated, respectively, as 75%, 98%, 100%, and %100 for *S. aureus.* The antimicrobial activity rates were 50%, 100%, 100%, and 100% for *B. subtilis*, in addition, 100%, 100% 100%, and 100% in *K. pneumoniae* and 72.4%, 97.52%, 100%, and 100% in *E. coli.* In well diffusion method, the diameter of inhibition zones formed with the increase of the concentration of AgNPs (65 nM, 130 nM, 195 nM, and 260 nM) was recorded as, respectively, 0, 28.7 ± 0.4, 46.3 ± 0.4, and 47.3 ± 0.6 mm in *S. aureus*; 0, 24.2 ± 0.1, 25.0, and 32.8 ± 0.4 mm in *B. subtilis*; 0, 13.0 ± 0.8, 25.7 ± 0.2, and 29.7 ± 0.3 mm in *K. pneumoniae*; and 0, 0, 27.7 ± 0.2, and 26.3 ± 0.3 mm in *E. coli* (Table S2). These results suggest that the inhibitory effect of AgNPs was more in gram-positive bacteria (*S. aureus* and *B. subtilis*) as compared with gram-negative bacteria (*K. pneumoniae* and *E. coli*). Gram-positive bacteria have an extra barrier of the outer membrane. Thus, gram-negative bacteria may be more resistant than gram-positive bacteria as is seen in our experiment results (Yeagle 2011).

In addition, growth effect of AgNPs in the corrosion setup showed that in the beginning (0 h), the number of the *H. variabilis* NOSK (ASW with no AgNPs) was 10^{10} CFU/mL. After 5-h corrosion experiments, bacterium was decreased to 10^5 CFU/mL (5 log) in the viable population of *H. variabilis* NOSK.

Coatings which contain antimicrobials were shown to inhibit microbial corrosion (Park et al. 2004) especially silver-based coatings which were effective in the inhibition of biofilm formation (Shah et al. 2019). However, it is really important to find the cytotoxic potential of the synthesized nanoparticles against cells. For this reason, biosynthesized AgNPs show dose-dependent cytotoxicity on HeLa cell lines. Cytotoxicity tests showed that 50% of the cells lose their viability at 120 μg/mL of AgNPs that dosage has been considered as IC50 for HeLa cells (Figure 5).

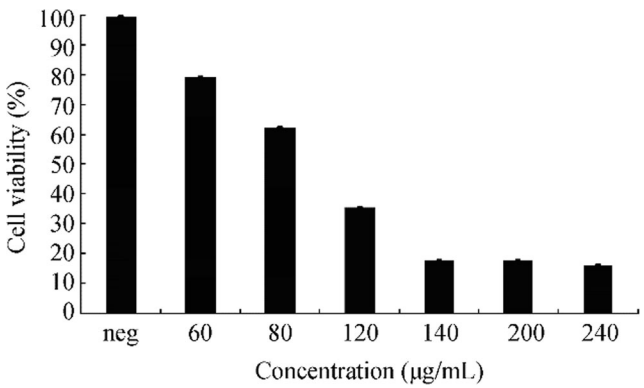

Figure 5 Biosynthesized silver nanoparticles properties of the cytotoxicity on HeLa cell lines

3.3 Weight Loss

The outcomes of the weight loss experiments for copper disks in the presence and absence of bacterial strain and AgNPs after 5-h immersion were presented in Table S3. In the absence of bacterial strains (abiotic control), the corrosion rate of the Cu disk was 0.01134 ± 0.001 mm y^{-1} (0.0029 mg ± 0.002). In the presence of *H. variabilis* NOSK, the corrosion rate of the Cu disk was 001564 ± 0.001 mm y^{-1} which is slightly higher (0.004 mg ± 0.002) than abiotic environment due to bacterial activity. However, in the presence of AgNPs, corrosion rate reached the lowest value of 0.00782 ± 0.002 mm y^{-1} (0.002 mg ± 0.002); therefore, the addition of AgNPs protected the Cu disk in the ASW. Similar results were also made by Narenkumar et al. (2018). According to the authors, corrosion rate in the presence of AgNPs synthesis from plant extract material was drastically reduced.

3.4 OCP, TAFEL, and Electrochemical Impedance Analysis

The potentiodynamic polarization curves of the ASW, ASW incubated with *H. variabilis* NOSK, and ASW with incubated *H. variabilis* NOSK + AgNPs after 5-h immersion are presented in Figure 6. The electrochemical parameters such as corrosion potential (E_{corr}), the corrosion current density (I_{corr}), anodic (β_a) and cathodic (β_c) Tafel values, and charge transfer values (R_{ct}) and solution resistance (R_s) values are presented in Table 1.

R_s represents the resistance of solution, R_p the resistance of passive film/biofilm pores, R_{ct} the resistance of charge transfer, Q_{CPE} the CPE parameters, Q_{dl} the CPE parameters for double layer, and η the dispersion parameters. The EIS measurements were carried out at 5-mV applied voltage at

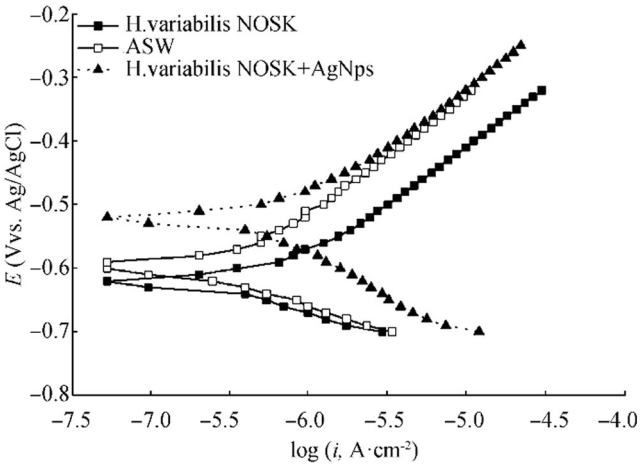

Figure 6 The potentiodynamic polarization curves of the ASW, ASW incubated with *H. variabilis* NOSK, and ASW with incubated *H. variabilis* NOSK + AgNPs after 5 h

Table 1 Electrochemical parameters of Cu corrosion inhibition in artificial seawater, artificial seawater inoculated with bacteria, and artificial seawater inoculated with bacteria + AgNPs

Systems	Polarization data						Impedance data					
	Eocp, *V*	E_{corr}, *V* vs Ag/AgCl	I_{corr}, μA cm^{-2}	Anodic Tafel slope β_a, *V* dec^{-1}	Cathodic Tafel slope $-\beta_c$, *V* dec^{-1}	R_s, Ω cm^2	R_p, Ω cm^2	R_{ct}, Ω cm^2	Q_{CPE} × 10^{-3}, Ω^{-1} cm^{-2}	η	Q_{dl} × 10^{-3}, Ω^{-1} cm^{-2}	η
Artificial seawater	− 0.451 ± 0.02	− 0.60 ± 0.02	5.30 ± 0.1	0.185 ± 0.1	0.103 ± 0.1	1.27 ± 0.01	681.43 ± 0.1	42431 ± 3	0.5 ± 0.01	0.49	0.47 ± 0.01	0.69
Halomonas variabilis NOSK	− 0.525 ± 0.01	− 0.62 ± 0.02	7.56 ± 0.1	0.076 ± 0.1	0.078 ± 0.1	3.39 ± 0.01	350.64 ± 0.1	3017.8 ± 2	37.08 ± 0.1	1	316.3 ± 2	0.66
Halomonas variabilis NOSK + AgNPs	− 0.406 ± 0.01	− 0.52 ± 0.02	3.13 ± 0.1	0.167 ± 0.1	0.186 ± 0.1	2.02 ± 0.01	22591 ± 0.1	172670 ± 3	829.2 ± 0.1	0.74	0.49 ± 0.1	0.6

sinusoidal wave in the frequency range of 20 kHz–50 mHz in pH 8.0 Artificial seawater at room temperature. All values are means of triplicate tests

Open circuit potential analysis is a nondestructive method to monitor the potential change on the surface of the metal/alloy. Table 1 shows that the OCP value of ASW was − 0.451 V vs Ag/AgCl, but after bacterium inoculation, OCP value slightly displaced toward more negative value (− 0.525 ± 0.01 V vs Ag/AgCl) which shows acceleration of corrosion. On the contrary, after addition of Ag nanoparticles, OCP value

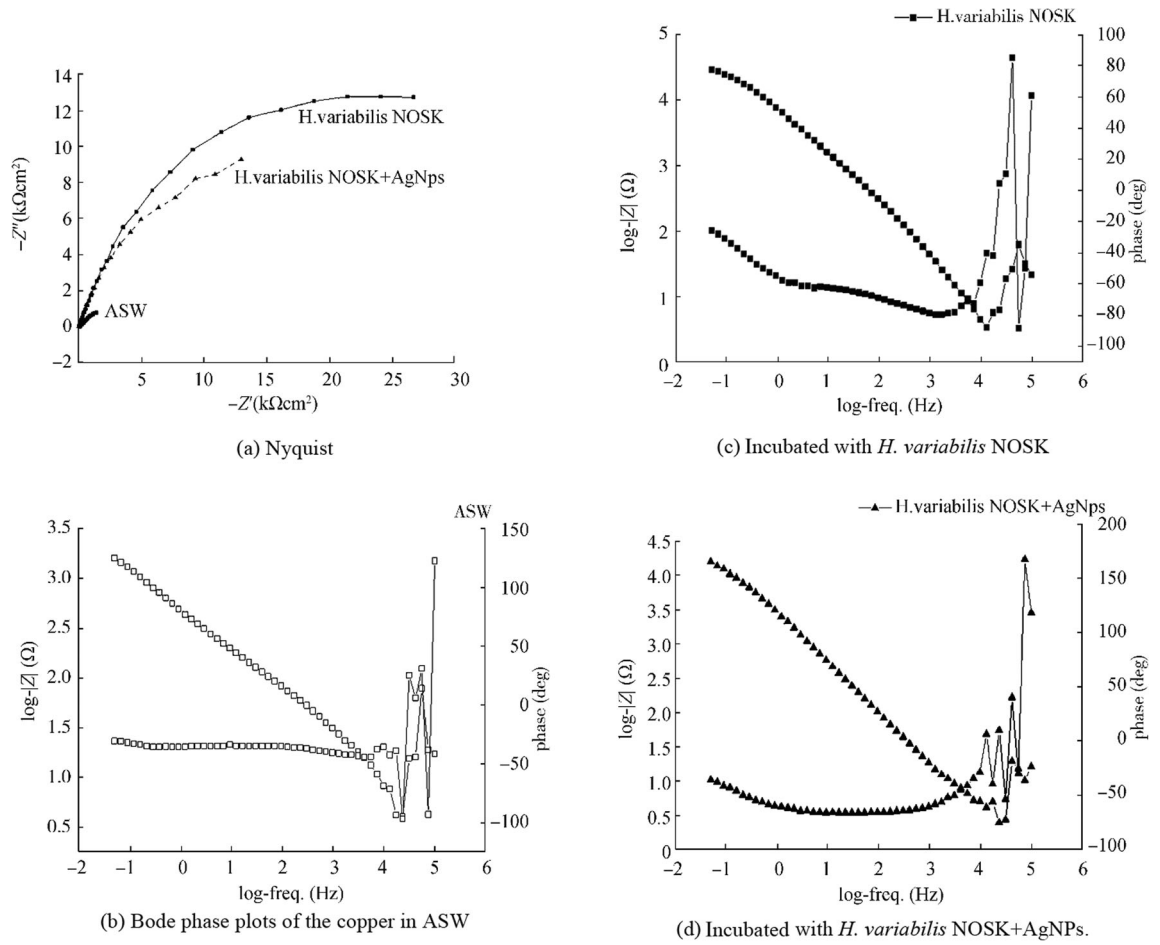

(a) Nyquist

(c) Incubated with *H. variabilis* NOSK

(b) Bode phase plots of the copper in ASW

(d) Incubated with *H. variabilis* NOSK+AgNPs.

Figure 7 Electrochemical impedance spectrum. (**a**) Nyquist. (**b**) Bode phase plots of the copper in ASW. (**c**) Incubated with *H. variabilis* NOSK. (d) Incubated with *H. variabilis* NOSK + AgNPs

was modified to more positive value (− 0.406 ± 0.01 V vs Ag/AgCl). It has been evident from the polarization curve that there was a remarkable potential shift to more positive values for copper in *H. variabilis* NOSK + AgNPs (− 0.52 ± 0.02 V vs Ag/AgCl) as compared to copper in ASW (− 0.60 ± 0.02 V vs Ag/AgCl) and copper in ASW after *H. variabilis* NOSK inoculation (− 0.62 ± 0.02 V vs Ag/AgCl). Furthermore, after 5 h of incubation, the corrosion current density (I_{corr}) in the presence of *H. variabilis* NOSK was higher than the ASW (5.30 ± 0.1 μA cm^{-2}), demonstrating that bacterium promoted Cu corrosion. As we expected, after adding AgNPs with bacterium, the corrosion current density began to decrease and reached the lowest value. Our results supported by earlier work of Preethi et al. (2019) investigated corrosion inhibition efficiency of zinc oxide nanoparticles (ZnONPs). In the presence of bacterium, I_{corr} was increased and it leads to the dissolution of copper ions on the metal surface. On the other hand, in the presence of ZnONPs, I_{corr} was reduced and the results reveal that nanoparticles form a protective film on the metal surface and thus inhibit the corrosion of Cu.

The interfacial phenomena of the biofilm formation and corrosion process development and characterization of the electrochemical reactions at the metal/biofilm interface are evaluated with EIS which is one of the most reliable methods (Yuan et al. 2013). In our study, EIS results confirmed with Tafel results. Nyquist plots of copper immersed in ASW, inoculated with *H. variabilis* NOSK and *H. variabilis* NOSK + AgNPs, are plotted in Figure 7a.

The entire frequency region can be divided into two sub-regions, corresponding to two time constants as shown in Bode plots (log|Z| vs. log(f)) in Figure 7b, c, and d (Bode phase plots of the copper in ASW (B), incubated with *H. variabilis* NOSK (C) and incubated with *H. variabilis* NOSK + AgNPs (D)). R_s is the solution resistance, R_f and Q_f are the resistance and the capacitance of the biofilm, respectively. R_{ct} and Q_{dl} correspond to a charge transfer resistance and a double-layered capacitance, respectively. The higher R_p values correspond to lower corrosion rates (Liu et al. 2017). The R_p value of copper in ASW was 681.43 ± 0.1 Ω cm^2 and after incubation, the R_p value decreases to 350.64 ± 0.1 Ω cm^2, indicating severe MIC attack caused by the biofilm/bacterium. However, in the presence of AgNPs, the R_p value increased to 172670 ± 3 Ω cm^2 which was significantly diminished. The calculated R_{ct} data represents the ability to hinder electron transfer between the surface and the substrate. Thus, the lower R_{ct} values in the ASW inoculated with *H. variabilis* NOSK mean the corrosion rate was higher (Zhou et al. 2018). On the contrary, the highest R_{ct} value was 172670 ± 3 Ω cm^2 in the ASW with *H. variabilis* NOSK + AgNPs. In addition, an electrical equivalent circuit comprised two time constants used to model the experimental values given in Figure 8.

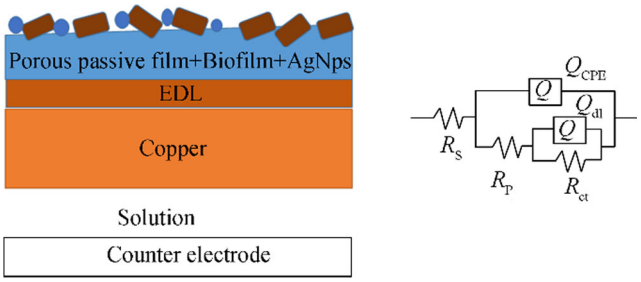

Figure 8 Schematic illustration and an electrical equivalent circuit of the biocorrosion mechanism by *H. variabilis* NOSK + AgNPs

The AgNPs' surface film on copper electrode after 5 h was investigated upon their electrochemical behavior in 50-mM phosphate buffer (pH 7.4) with cyclic voltammetry in Figure 9. As can be seen from Figure 9, two characteristic peaks of Ag were observed after 5-h corrosion test. An oxidation peak corresponding to Ag to Ag^+ oxidation was observed with a peak potential of 0.178 V and a peak current of 13.8 mA, while on the reverse scan, a reduction peak appeared at − 0.129 V with a peak current of 15.97 mA. These two peaks were not observed at the bare copper electrode as expected. In addition, the absence of copper peak after 5-h corrosion showed that the surface was completely covered with silver nanoparticles. Thus, it can be said from the obtained voltammograms that the silver nanoparticles were adsorbed on the copper electrode surface from the corrosion solution (Palisoc et al. 2018).

4 Conclusions

In conclusion, due to adverse effects of the chemical and physical nanoparticles' synthesis methods, new and novel sustainable methods sought for the discovery. In this study, the biosynthesis of silver nanoparticles by the *Lysinibacillus* sp.

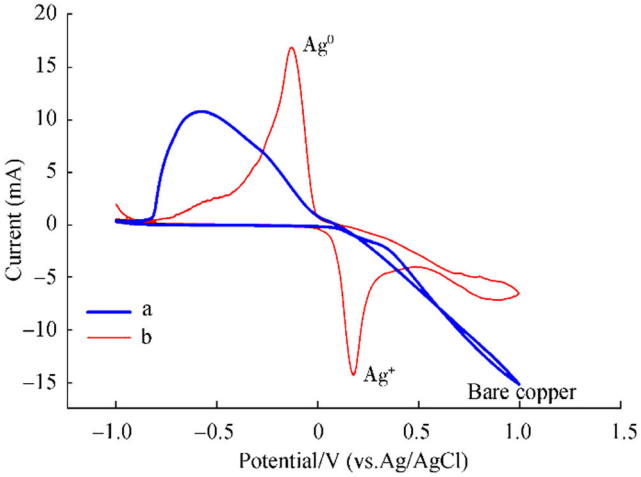

Figure 9 Cyclic voltammograms. (**a**) Bare Cu electrode and (**b**) the copper electrode with AgNPs after 5-h corrosion at a scan rate of 100 mV/s in pH 7.4 phosphate buffer solution

NOSK bacteria is demonstrated. Biosynthesis of AgNPs is confirmed by using UV-Vis absorption, transmission electron microscopy (TEM), and Fourier transform infrared spectroscopy (FTIR). The average crystalline size and shape of the nanoparticles were 42 nm and spherical in shape, respectively.

In application, these nanoparticles exhibited efficient antimicrobial activity against gram-positive and gram-negative bacteria. In addition, the inhibition of halophilic bacterium's biocorrosion on copper in marine environment was successfully evaluated in detail in this work. The EIS analysis showed increased R_p value for bacterium with AgNPs corresponding to lower corrosion rates. For this reason, biosynthesized AgNPs are used as an active antimicrobial corrosion inhibitor and these non-toxic nanoparticles have a potential to be used as antibacterial paints and coatings due to long-term protection property especially in marine industry.

Funding This research is funded by the Scientific and Technological Research Council of Turkey (TÜBITAK, Project MAG#218 M508).

Supplementary Information The online version of this article (https://doi.org/10.1007/s11804-020-00188-6) contains supplementary material, which is available to authorized users.

References

Abdolahi A, Hamzah E, Ibrahim Z, Hashim S (2014) Microbially influenced corrosion of steels by *Pseudomonas aeruginosa*. Corros Rev 32(3-4):129–141. https://doi.org/10.1515/corrrev-2013-0047

Arulmozhi V, Pandian K, Mirunalini S (2013) Ellagic acid encapsulated chitosan nanoparticles for drug delivery system in human oral cancer cell line (KB). Colloids Surf B: Biointerfaces, 110, 313-320. https://doi.org/10.1016/j.colsurfb.2013.03.039

Baygar T, Sarac N, Ugur A, Karaca IR (2019) Antimicrobial characteristics and biocompatibility of the surgical sutures coated with biosynthesized silver nanoparticles. Bioorg Chem 86:254–258. https://doi.org/10.1016/j.bioorg.2018.12.034

Bhaumik J, Gogia G, Kirar S, Vijay L, Thakur NS, Banerjee UC, Laha JK (2016) Bioinspired nanophotosensitizers: synthesis and characterization of porphyrin–noble metal nanoparticle conjugates. New J Chem 40(1):724–731. https://doi.org/10.1039/C5NJ02056E

Brauer JI, Celikkol-Aydin S, Sunner JA, Gaylarde CC, Beech IB (2017) Metabolomic imaging of a quaternary ammonium salt within a marine bacterial biofilm on carbon steel. Int Biodeterior Biodegradation 125:33–36. https://doi.org/10.1016/j.ibiod.2017.08.007

Cao H (2017) Silver nanoparticles for antibacterial devices: biocompatibility and toxicity. CRC Press https://doi.org/10.1201/9781315370569

Chandra K, Mahanti A, Singh AP, Kain V, Gujar HG (2019) Microbiologically influenced corrosion of 70/30 cupronickel tubes of a heat-exchanger. Eng Fail Anal 105:1328–1339. https://doi.org/10.1016/j.engfailanal.2019.08.005

Chen S, Zhang D (2018) Study of corrosion behavior of copper in 3.5 wt.% NaCl solution containing extracellular polymeric substances of an aerotolerant sulphate-reducing bacteria. Corros Sci 136:275–284. https://doi.org/10.1016/j.corsci.2018.03.017

Fayaz AM, Balaji K, Girilal M, Yadav R, Kalaichelvan PT, Venketesan R (2010) Biogenic synthesis of silver nanoparticles and their synergistic effect with antibiotics: a study against gram-positive and gram-negative bacteria. Biol Med 6(1):103–109. https://doi.org/10.1016/j.nano.2009.04.006

Firdhouse MJ, Lalitha P (2015) Biosynthesis of silver nanoparticles and its applications. J Nanotechnol pp 1–18. https://doi.org/10.1155/2015/829526

George RP, Muraleedharan P, Sreekumari KR, Khatak HS (2003) Influence of surface characteristics and microstructure on adhesion of bacterial cells onto a type 304 stainless steel. Biofouling 19(1):1–8. https://doi.org/10.1080/08927010290031017

Giovanni M, Pumera M (2012) Size dependant electrochemical behavior of silver nanoparticles with sizes of 10, 20, 40, 80 and 107 nm. Electroanalysis 24(3):615–617. https://doi.org/10.1002/elan.201100690

Gou Y, Zhou R, Ye X, Gao S, Li X (2015) Highly efficient in vitro biosynthesis of silver nanoparticles using *Lysinibacillus sphaericus* MR-1 and their characterization. Sci Technol Adv Mater 16(1):015004. https://doi.org/10.1088/1468-6996/16/1/015004

Hebbalalu D, Lalley J, Nadagouda MN, Varma RS (2013) Greener techniques for the synthesis of silver nanoparticles using plant extracts, enzymes, bacteria, biodegradable polymers, and microwaves. ACS Sustain Chem Eng 1(7):703–712. https://doi.org/10.1021/sc4000362

Huang Y, Peng X, Chen XQ (2019) TiO_2 nanoparticles-assisted α-Al_2O_3 direct thermal growth on nickel aluminide intermetallics: template effect of the oxide with the hexagonal oxygen sublattice. Corros Sci 153:109–117. https://doi.org/10.1016/j.corsci.2019.03.025

Jia R, Unsal T, Xu D, Lekbach Y, Gu T (2019) Microbiologically influenced corrosion and current mitigation strategies: a state of the art review. Int Biodeterior Biodegradation 137:42–58. https://doi.org/10.1016/j.ibiod.2018.11.007

Kailasa SK, Park TJ, Rohit JV. Koduru JR (2019) Antimicrobial activity of silver nanoparticles. *In Nanoparticles in Pharmacotherapy*, 461-484. https://doi.org/10.1016/B978-0-12-816504-1.00009-0

Kardas M, Gozen AG, Severcan F (2014) FTIR spectroscopy offers hints towards widespread molecular changes in cobalt-acclimated freshwater bacteria. Aquat Toxicol 155:15–23. https://doi.org/10.1016/j.aquatox.2014.05.027

Kim JS, Kuk E, Yu KN, Kim JH, Park SJ, Lee HJ, Kim YK (2007) Antimicrobial effects of silver nanoparticles. Nanomedicine 3(1):95–101. https://doi.org/10.1016/j.nano.2006.12.001

Kip N, Van Veen JA (2015) The dual role of microbes in corrosion. ISME J 9(3):542–551. https://doi.org/10.1038/ismej.2014.169

Li X, Zhang D, Liu Z, Li Z, Du C, Dong C (2015) Materials science: share corrosion data. Nature 527(7579):441–442. https://doi.org/10.1038/527441a

Little BJ, Lee JS (2007) Microbiologically influenced corrosion (Vol. 3). John Wiley & Sons. https://doi.org/10.1002/047011245X

Liu H, Cheng YF (2018) Mechanistic aspects of microbially influenced corrosion of X52 pipeline steel in a thin layer of soil solution containing sulphate-reducing bacteria under various gassing conditions. Corros Sci 133:178–189. https://doi.org/10.1016/j.corsci.2018.01.029

Liu H, Gu T, Lv Y, Asif M, Xiong F, Zhang G, Liu H (2017) Corrosion inhibition and anti-bacterial efficacy of benzalkonium chloride in artificial CO_2-saturated oilfield produced water. Corros Sci 117:24–34. https://doi.org/10.1016/j.corsci.2017.01.006

Liu T, Wang Y, Pan S, Zhao Q, Zhang C, Gao S, Guo Z, Guo N, Sand W, Chang X, Dong L, Yin Y (2019) The addition of copper accelerates the corrosion of steel via impeding biomineralized film formation of

Bacillus subtilis in seawater. Corros Sci 149:153–163. https://doi.org/10.1016/j.corsci.2019.01.010

Maharubin S, Nayak C, Phatak O, Kurhade A, Singh M, Zhou Y, Tan G (2019) Polyvinylchloride coated with silver nanoparticles and zinc oxide nanowires for antimicrobial applications. Mater Lett 249:108–111. https://doi.org/10.1016/j.matlet.2019.04.058

Mittal AK, Bhaumik J, Kumar S, Banerjee UC (2014) Biosynthesis of silver nanoparticles: elucidation of prospective mechanism and therapeutic potential. J Colloid Interface Sci 415:39–47. https://doi.org/10.1016/j.jcis.2013.10.018

Moradi M, Ye S, Song Z (2019) Dual role of *Pseudoalteromonas piscicida* biofilm for the corrosion and inhibition of carbon steel in artificial seawater. Corros Sci 152:10–19. https://doi.org/10.1016/j.corsci.2019.02.025

Narenkumar J, Parthipan P, Madhavan J, Murugan K, Marpu SB, Suresh AK, Rajasekar A (2018) Bioengineered silver nanoparticles as potent anti-corrosive inhibitor for mild steel in cooling towers. Environ Sci Pollut Res 25(6):5412–5420. https://doi.org/10.1007/s11356-017-0768-6

Nayak RR, Pradhan N, Behera D, Pradhan KM, Mishra S, Sukla LB, Mishra BK (2011) Green synthesis of silver nanoparticle by *Penicillium purpurogenum* NPMF: the process and optimization. J Nanopart Res 13(8):3129–3137. https://doi.org/10.1007/s11051-010-0208-8

Otari SV, Patil RM, Ghosh SJ, Thorat ND, Pawar SH (2015) Intracellular synthesis of silver nanoparticle by actinobacteria and its antimicrobial activity. Spectrochim Acta A Mol Biomol Spectrosc 136:1175–1180. https://doi.org/10.1016/j.saa.2014.10.003

Ou HH, Tran QTP, Lin PH (2018) A synergistic effect between gluconate and molybdate on corrosion inhibition of recirculating cooling water systems. Corros Sci 133:231–239. https://doi.org/10.1016/j.corsci.2018.01.014

Palisoc ST, Natividad MT, De Jesus N, Carlos J (2018) Highly sensitive AgNP/MWCNT/Nafion modified GCE-based sensor for the determination of heavy metals in organic and non-organic vegetables. Sci Rep 8(1):1–13. https://doi.org/10.1038/s41598-018-35781-x

Park SI, Daeschel MA, Zhao Y (2004) Functional properties of antimicrobial lysozyme-chitosan composite films. J Food Sci 69:M215–M221. https://doi.org/10.1111/j.1365-2621.2004.tb09890.x

Parthipan P, Babu TG, Anandkumar B, Rajasekar A (2017) Biocorrosion and its impact on carbon steel API 5LX by *Bacillus subtilis* A1 and *Bacillus cereus* A4 isolated from Indian crude oil reservoir. J Bio-Tribo-Corros 3(3):32. https://doi.org/10.1007/s40735-017-0091-2

Peszke J, Nowak A, Szade J, Szurko A, Zygadło D, Michałowska M, Ostafin MM (2016) Effect of silver/copper and copper oxide nanoparticle powder on growth of Gram-negative and Gram-positive bacteria and their toxicity against the normal human dermal fibroblasts. J Nanopart Res 18(12):355. https://doi.org/10.1007/s11051-016-3671-z

Poulios I, Spathis P, Grigoriadou A, Delidou K, Tsoumparis P (1999) Protection of marbles against corrosion and microbial corrosion with TiO_2 coatings. J Environ Sci Health Part A 34(7):1455–1471. https://doi.org/10.1080/10934529909376905

Preethi PS, Narenkumar J, Prakash AA, Abilaji S, Prakash C, Rajasekar A, Nanthini AUR, Valli G (2019) Myco-synthesis of zinc oxide nanoparticles as potent anti-corrosion of copper in cooling towers. J Clust Sci 30(6):1583–1590. https://doi.org/10.1007/s10876-019-01600-0

San Keskin NO, Celebioglu A, Sarioglu OF, Ozkan AD, Uyar T, Tekinay T (2015) Removal of nanofibrous web. RSC Adv 5(106):86867–86874. https://doi.org/10.1039/C5RA15601G

San Keskin NO, Koçberber Kılıç N, Dönmez G, Tekinay T (2016) Green synthesis of silver nanoparticles using cyanobacteria and evaluation of their photocatalytic and antimicrobial activity. Int J Nano Res 40:120–127. https://doi.org/10.4028/www.scientific.net/JNanoR.40.120

San NO, Nazır H, Dönmez G (2012a) Microbiologically influenced corrosion of NiZn alloy coatings by *Delftia acidovorans* bacterium. Corros Sci 64:198–203. https://doi.org/10.1016/j.corsci.2012.07.021

San NO, Nazır H, Dönmez G (2012b) Microbiologically influenced corrosion failure analysis of nickel–copper alloy coatings by *Aeromonas salmonicida* and *Delftia acidovorans* bacterium isolated from pipe system. Eng Fail Anal 25:63–70. https://doi.org/10.1016/j.engfailanal.2012.04.007

Shah S, Gaikwad S, Nagar KS, Vaidya V, Nawani N, Pawar S (2019) Biofilm inhibition and anti-quorum sensing activity of phytosynthesized silver nanoparticles against the nosocomial pathogen *Pseudomonas aeruginosa*. Biofouling 35(1):34–49. https://doi.org/10.1080/08927014.2018.1563686

Shahverdi AR, Minaeian, Shahverdi HR, Jamalifar H, Nohi AA (2007) Rapid synthesis of silver nanoparticles using culture supernatants of Enterobacteria: a novel biological approach. Process Biochem 42(5):919–923. https://doi.org/10.1016/j.procbio.2007.02.005

Sondi I, Salopek-Sondi B (2004) Silver nanoparticles as antimicrobial agent: a case study on *E. coli* as a model for Gram-negative bacteria. J Colloid Interface Sci 275(1):177–182. https://doi.org/10.1016/j.jcis.2004.02.012

Starosvetsky J, Starosvetsky D, Armon R (2007) Identification of microbiologically influenced corrosion (MIC) in industrial equipment failures. Eng Fail Anal 14(8):1500–1511. https://doi.org/10.1016/j.engfailanal.2007.01.020

Thakur NS, Bhaumik J, Kirar S, Banerjee UC (2017) Development of gold-based phototheranostic nanoagents through a bioinspired route and their applications in photodynamic therapy. ACS Sustain Chem Eng 5(9):7950–7960. https://doi.org/10.1021/acssuschemeng.7b01501

Videla HA, Herrera LK (2009) Understanding microbial inhibition of corrosion. A comprehensive overview. Int Biodeterior Biodegradation 63(7):896–900. https://doi.org/10.1016/j.ibiod.2009.02.002

Videla HA, de Mele MFL, Brankevich G (1988) Technical note: assessment of corrosion and microfouling of several metals in polluted seawater. Corrosion 44(7):423–426. https://doi.org/10.5006/1.3583957

Wang W, Li X, Wang J, Xu H, Wu J (2004) Influence of biofilms growth on corrosion potential of metals immersed in seawater. Mater Corros 55(1):30–35. https://doi.org/10.1002/maco.200303690

Wang H, Ju LK, Castaneda H, Cheng G, Newby BMZ (2014) Corrosion of carbon steel C1010 in the presence of iron oxidizing bacteria *Acidithiobacillus ferrooxidans*. Corros Sci 89:250–257. https://doi.org/10.1016/j.corsci.2014.09.005

Xu D, Xia J, Zhou E, Zhang D, Li H, Yang C, Yang K (2017) Accelerated corrosion of 2205 duplex stainless steel caused by marine aerobic *Pseudomonas aeruginosa* biofilm. Bioelectrochemistry 113:1–8. https://doi.org/10.1016/j.bioelechem.2016.08.001

Ye J, Hu D, Yin J, Huang W, Xiang R, Zhang L, Wang X, Han J, Chen GQ (2020) Stimulus response-based fine-tuning of polyhydroxyalkanoate pathway in Halomonas. Metab Eng 57:85–95. https://doi.org/10.1016/j.ymben.2019.10.007

Yeagle PL (2011) *The structure of biological membranes*. CRC press https://doi.org/10.1201/b11018

Yuan S, Liang B, Zhao Y, Pehkonen SO (2013) Surface chemistry and corrosion behaviour of 304 stainless steel in simulated seawater containing inorganic sulphide and sulphate-reducing bacteria. Corros Sci 74:353–366. https://doi.org/10.1016/j.corsci.2013.04.058

Zhou E, Li H, Yang C, Wang J, Xu D, Zhang D, Gu T (2018) Accelerated corrosion of 2304 duplex stainless steel by marine *Pseudomonas aeruginosa* biofilm. Int Biodeterior Biodegradation 127:1–9. https://doi.org/10.1016/j.ibiod.2017.11.00